

Current Loop Control of Jet Fan Motors in Thu Thiem Tunnel by the Exact Linearization Method

An Thi Hoai Thu Anh

Department of Electrical Engineering, University of Transport and Communications, Vietnam
htanh.ktd@utc.edu.vn (corresponding author)

Tran Van Khoi

Department of Electrical Engineering, University of Transport and Communications, Vietnam
tvkhai.ktd@utc.edu.vn

Lam Quang Thai

Department of Electrical Engineering, University of Transport and Communications, Vietnam
thailq_ph@utc.edu.vn

Received: 30 November 2023 | Revised: 3 March 2024 | Accepted: 5 March 2024

Licensed under a CC-BY 4.0 license | Copyright (c) by the authors | DOI: <https://doi.org/10.48084/etasr.6686>

ABSTRACT

The Thu Thiem road tunnel located deep under the Saigon River is currently ventilated by a system of 12 jet fans that push dust and dirty air out into the environment. These jet fans are driven by Induction Motors (IMs) modeled by mathematical equations on the structural nonlinear dq coordinate system, so the conventional linear controllers partly fail to meet the response requirements. Therefore, this paper proposes the application of the exact linearization control method for the current loop in the Field Oriented Control (FOC) structure of an IM that drives a jet fan of the Thu Thiem road tunnel. This is a control method based on a linearization model with cascaded loops. The stator current controller controls two currents: i_{sd} controls the flux, and i_{sq} controls the torque. The control design is verified by the simulation results on Matlab/Simulink with data collected from the jet fan system of the Thu Thiem road tunnel.

Keywords-road tunnel ventilation; Thu Thiem road tunnel; exact linearization; Field Oriented Control (FOC); Induction Motor (IM)

I. INTRODUCTION

Ventilation system of road tunnels plays an important role in maintaining a comfortable and safe driving environment by expelling toxic gases out of the tunnel, such as CO, CO₂, and NO₂, released by vehicles circulating in the tunnel [1-3]. In addition, in emergency situations such as fire and explosions [4-7], the ventilation system helps control the smoke and save people so that the tunnel quickly returns to normal operation [8]. Tunnel ventilation methods are divided into natural ventilation and mechanical ventilation [3]. Mechanical ventilation methods are further divided into vertical, semi-horizontal, and horizontal. Due to the geographical location and structure of Thu Thiem tunnel connecting District 1 with District 2 of Ho Chi Minh City, and its length of 1490 m and depth under the Saigon River bed, Thu Thiem tunnel uses the vertical ventilation vertical ventilation [9]. In a vertical ventilation system, jet fans are installed at certain intervals to [10-11]. The layout diagram of jet fans in Thu Thiem tunnel is

shown in Figure 1. The jet fans in the Thu Thiem tunnel are operating in on-off mode, but the concentration of exhaust gases in the tunnel changes during its operation, so controlling the jet fan system at different speeds in order to save energy should be considered.

Adjusting the jet fan speed by the Field Oriented Control (FOC) method for Induction Motors (IMs) is widely utilized in industry and transportation [12] due to advantages such as mobilizing good torque even at low speeds. In the control structure of induction motor on the dq coordinate system, the current i_{sd} controls the flux, and the current i_{sq} controls the torque. In order to design the controllers to ensure the stability of the system, there are linear control methods such as the PI controller or PI combined with optimization algorithms [13-14], ADRC controller [15], deadbeat [16] or nonlinear controllers such as the exact linearization, sliding mode, backstepping, neuron, robust nonlinear predictive control [17-24], etc.

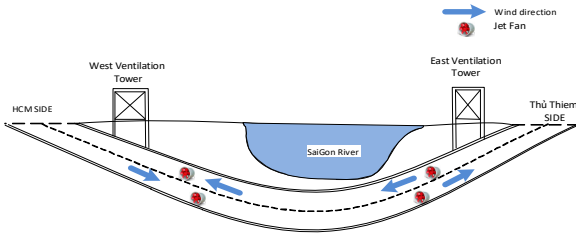


Fig. 1. Ventilation diagram of Thu Thiem road tunnel.

The typical linear control method is the PI controller, which has the advantage of simple design and little dependence on motor parameters. However, the PI controller only achieves best performance around the balanced operating point. If the motor parameters change during operation, or the load changes drastically, the dynamic response and quality of the drive system will be degraded. In equations, the modeled IM, shows bilinear nonlinearity by the product $\omega_s i_{sd}$, $\omega_s i_{sq}$. Therefore, it is necessary to design controllers by nonlinear methods.

The proposed linearization method for the current loop uses state feedback to convert a system of nonlinear current equations into a linear input-output relationship. That is, from the nonlinear model of the object to a new system with a linear model in the entire state space. On the new coordinate system, the input and output relations are completely isolated, so two currents i_{sd} , i_{sq} can be controlled independently by the input variables w_d and w_q . From there, we can design the current controllers according to the direct channel separation structure and evaluate them by the linear control theory.

II. MODELING OF THE JET FAN SYSTEM

The control structure of the jet fan is shown in Figure 2, including the inverter and the IM driving the jet fan, CO and vision sensors, and the PLC. In this section, focus is given on the controlling drive system.

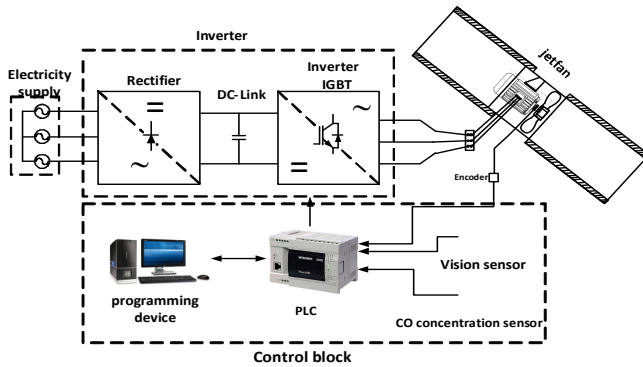


Fig. 2. Jet fan control structure.

A. Induction Motor Modeling

The equation group (1) describes the mathematics of the asynchronous motor on the $d-q$ coordinate system [25], where $\psi'_{rd} = \psi_{rd} / L_m$ and $\psi'_{rq} = \psi_{rq} / L_m$, $\sigma = 1 - L_m^2 / (L_s L_r)$ is the total dissipation factor, $T_s = L_s / L_r$ is the stator time constant,

$T_r = L_r / R_r$ is the rotor time constant, i_{sd} , i_{sq} , u_{sd} , u_{sq} denote the stator current and voltage on the dq coordinate system, ω_s is the angular speed of stator flux, m_M is the motor torque, m_L is the load torque, and z_p is the number of poles.

$$\begin{cases} \frac{di_{sd}}{dt} = -\left(\frac{1}{\sigma T_s} + \frac{1-\sigma}{\sigma T_r}\right)i_{sd} + \omega_s i_{sq} + \frac{1-\sigma}{\sigma T_r}\psi'_{rd} \\ + \frac{1-\sigma}{\sigma}\omega\psi'_{rq} + \frac{1}{\sigma L_s}u_{sd} \\ \frac{di_{sq}}{dt} = -\left(\frac{1}{\sigma T_s} + \frac{1-\sigma}{\sigma T_r}\right)i_{sq} - \omega_s i_{sd} + \frac{1-\sigma}{\sigma T_r}\psi'_{rq} \\ - \frac{1-\sigma}{\sigma}\omega\psi'_{rd} + \frac{1}{\sigma L_s}u_{sq} \\ \frac{d\psi_{rd}}{dt} = \frac{L_m}{T_r}i_{sd} - \frac{1}{T_r}\psi_{rd} + (\omega_s - \omega)\psi_{rq} \\ \frac{d\psi_{rq}}{dt} = \frac{L_m}{T_r}i_{sq} - (\omega_s - \omega)\psi_{rd} - \frac{1}{T_r}\psi_{rq} \\ m_M = \frac{3}{2}z_p \frac{L_m^2}{L_r}\psi'_{rd}i_{sd} = \frac{3}{2}z_p(1-\sigma)L_s\psi'_{rd}i_{sd} \\ m_M = m_L + \frac{J}{z_p}\frac{d\omega}{dt} \\ \theta_s = \theta_0 + \int \omega_s dt \end{cases} \quad (1)$$

B. Jet Fan Load Characteristic

The calculation and selection of the drive motor and control method depends on the working load characteristics. The characteristic of the fan load is described by [25]:

$$M_c = M_{rated} \left(\frac{\omega}{\omega_{rated}}\right)^2 \quad (2)$$

where M_{rated} is the torque corresponding to the rated speed ω_{dm} and M_c is the torque with speed ω . The characteristic curve is shown in Figure 3.

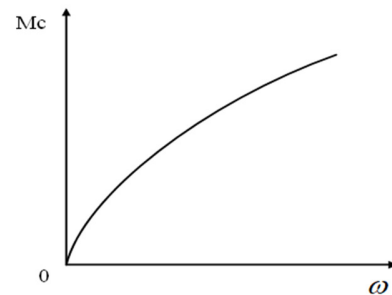


Fig. 3. Mechanical characteristics of the jet fan.

III. JET FAN DRIVE CONTROL DESIGN

The FOC structure is given in Figure 4. Three loops need to be designed: current loop, flux loop, and speed loop.

A. Design of the Current Loop by the Exact Linearization Method

The current loop is designed to require the fast, exact, decoupling responses, between the currents i_{sd} and i_{sq} . From (1), temporary variables and parameters are denoted as follows:

$$a = \frac{1}{\sigma L_s}; b = \frac{1}{\sigma T_s}; c = \frac{1-\sigma}{\sigma T_r}; d = b + c$$

State variables: $x_1 = i_{sd}; x_2 = i_{sq}; x_3 = \theta_s$

Input variables: $u_1 = u_{sd}; u_2 = u_{sq}; u_3 = \omega_s$

Output variables: $y_1 = i_{sd}; y_2 = i_{sq}; y_3 = \theta_s$

Equation (1) is rewritten as:

$$\begin{cases} \frac{dx_1}{dt} = -dx_1 + x_2u_3 + au_1 + c\psi'_{rd} \\ \frac{dx_2}{dt} = -dx_2 - x_1u_3 + au_2 - cT_r\omega\psi'_{rd} \\ \frac{dx_3}{dt} = u_3 \end{cases} \quad (3)$$

State coordinate system transformation is performed:

$$z = \begin{bmatrix} z_1 \\ z_2 \\ z_3 \end{bmatrix} = \begin{bmatrix} m_1^1(x) \\ m_1^2(x) \\ m_1^3(x) \end{bmatrix} = \begin{bmatrix} g_1(x) \\ g_2(x) \\ g_3(x) \end{bmatrix} = \begin{bmatrix} x_1 \\ x_2 \\ x_3 \end{bmatrix} \quad (4)$$

The result of the coordinate conversion is:

$$\begin{cases} \frac{dz_1}{dt} = -dx_1 + c\psi'_{rd} + au_1 + x_2u_3 = w_1 \\ \frac{dz_2}{dt} = -dx_2 - cT_r\omega\psi'_{rd} + au_2 - x_1u_3 = w_2 \\ \frac{dz_3}{dt} = u_3 = w_3 \end{cases} \quad (5)$$

Vector ω is calculated by:

$$\begin{cases} \frac{dz_1}{dt} = -dx_1 + c\psi'_{rd} + au_1 + x_2u_3 = w_1 \\ \frac{dz_2}{dt} = -dx_2 - cT_r\omega\psi'_{rd} + au_2 - x_1u_3 = w_2 \\ \frac{dz_3}{dt} = u_3 = w_3 \end{cases} \quad (6)$$

and has the form: $w = p(x) + L(x)u$.

Gas ω is the new input variable vector, and the state feedback control law is specifically calculated as follows:

$$u = -L^{-1}(x)p(x) + L^{-1}(x)\omega$$

After calculations, we get (7) which is equivalent to (8):

$$u = \begin{bmatrix} u_1 \\ u_2 \\ u_3 \end{bmatrix} = \begin{bmatrix} \frac{dx_1}{a} - \frac{c\psi'_{rd}}{a} \\ \frac{dx_2}{a} + \frac{cT_r\omega\psi'_{rd}}{a} \\ 0 \end{bmatrix} + \begin{bmatrix} \frac{1}{a} & 0 & -x_2 \\ 0 & \frac{1}{a} & x_1 \\ 0 & 0 & 1 \end{bmatrix} \begin{bmatrix} \omega_1 \\ \omega_2 \\ \omega_3 \end{bmatrix} \quad (7)$$

$$\begin{cases} U_{sd} = \frac{1}{a}(w_1 + dx_1 - c\psi'_{rd} - x_2w_3) \\ U_{sq} = \frac{1}{a}(w_2 + dx_2 + x_1w_3 + cT_r\omega\psi'_{rd}) \\ \theta_s = w_3 \end{cases} \quad (8)$$

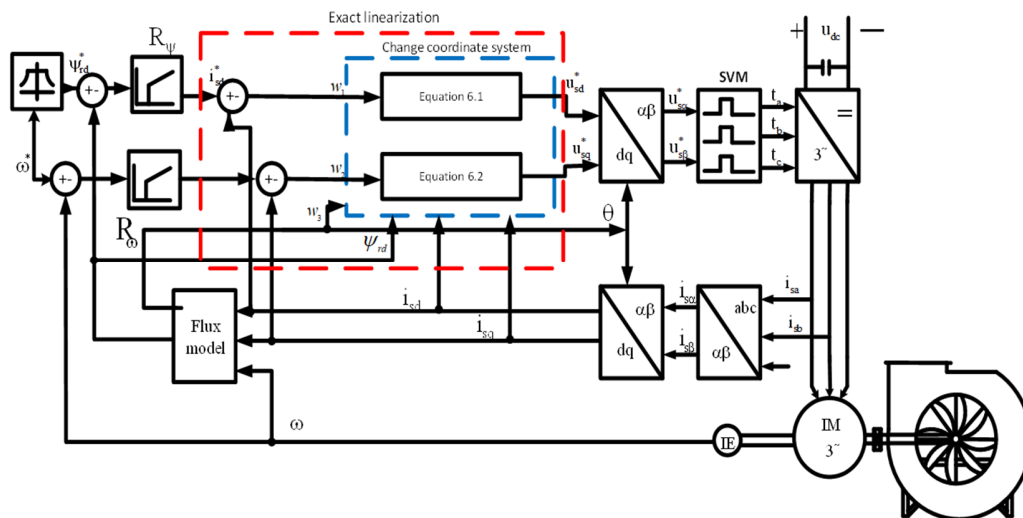


Fig. 4. Diagram of directional control according to rotor flux.

B. Design of a Magnetic Flux Loop

The flux controller produces a magnetizing current that provides a set value for the current controller. Since the R_{i_s} series controller is fast, accurate, and non-interactive, we can assume that the R_{i_s} series is a 1-to-1 link. Equation (9) is derived from the rotor flux equation on the dq domain:

$$\dot{\phi}_{rd} = \frac{i_{sd} L_m}{sT_r + 1} \tag{9}$$

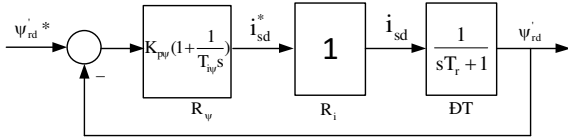


Fig. 5. Structure of the rotor flux controller ψ_{rd} .

$T_{i\psi} = T_r$ was chosen to eliminate the time constant. The object's open-system transfer function is:

$$F_h(s) = \frac{k_{p\psi}}{T_{i\psi} \cdot s} \tag{10}$$

The closed system transfer function is:

$$F_k(s) = \frac{F_h(s)}{1 + F_h(s)} = \frac{\frac{k_{p\psi}}{T_{i\psi} \cdot s}}{1 + \frac{k_{p\psi}}{T_{i\psi} \cdot s}} = \frac{l}{T_{k\psi} \cdot s + l} \tag{11}$$

The transfer function is an integral of order 1. The time constant of the closed-system transfer function R_ψ was chosen to be an integer times the time constant of the set R_{i_s} : $T_{k\psi} = nT_{ki}$ for $n=5$. The calculated number is substituted to get the $k_{p\psi}, T_{i\psi}$ parameters of the flux regulator.

C. Speed Loop Design

Since the R_{i_s} series controller is fast, accurate, and non-interactive, we can assume that the R_{i_s} set is a 1-to-1 link. Starting from the moment equation:

$$m_M = m_t + \frac{J}{z_p} \frac{d\omega}{dt} \tag{12}$$

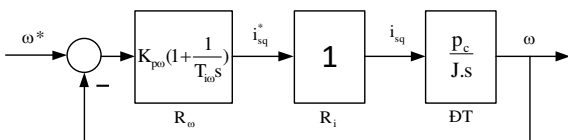


Fig. 6. Controller structure R_ω .

The open system transfer function is:

$$F_{h\omega}(s) = \frac{k_{p\omega}(I + T_{i\omega}s)}{T_{i\omega}s} \cdot \frac{z_p}{J \cdot s} = \frac{k_{p\omega} \cdot z_p}{T_{i\omega} \cdot J} \cdot \frac{I + T_{i\omega} \cdot s}{s^2} \tag{13}$$

We choose:

$$k_l = \frac{K_{p\omega} P_c}{J T_{i\omega}} \rightarrow F_h = \frac{k_l(T_{i\omega}s + I)}{s}$$

The closed system transfer function is:

$$F_{k\omega}(s) = \frac{F_{h\omega}(s)}{1 + F_{h\omega}(s)} = \frac{k_l \frac{I + T_{i\omega} \cdot s}{s^2}}{1 + k_l \frac{I + T_{i\omega} \cdot s}{s^2}} = \frac{k_l(I + T_{i\omega} \cdot s)}{s^2 + k_l(I + T_{i\omega} \cdot s)} = \frac{k_l \cdot T_{i\omega} \cdot s + k_l}{s^2 + k_l \cdot T_{i\omega} \cdot s + k_l} \tag{14}$$

The speed controller is designed according to the optimal standard and symmetrical with the standard function:

$$G_K(s) = \frac{2\varepsilon\omega_n s + \omega_n^2}{s^2 + 2\varepsilon\omega_n s + \omega_n^2} \tag{15}$$

where ω_n is the natural frequency of the oscillation and ε is the damping coefficient of the oscillation ($0 < \varepsilon < 1$).

The time for the output value to be within 2% of the set value is t_s .

$$\Rightarrow \begin{cases} k_l = \omega_n^2 \\ k_l \cdot T_{i\omega} = 2 \cdot \varepsilon \cdot \omega_n \end{cases} \Leftrightarrow \begin{cases} k_{p\omega} = \frac{\omega_n^2 \cdot T_{i\omega} \cdot J}{z_p} \\ T_{i\omega} = \frac{2 \cdot \varepsilon}{\omega_n} \end{cases} \tag{16}$$

The calculated number is substituted to obtain the $k_{p\omega}, T_{i\omega}$ parameters of the speed regulator.

IV. SIMULATION RESULTS

Simulations conducted on Matlab/Simulink software with a current regulator that is an exact linearization method and the outer PI loop controls.

TABLE I. JETFAN PARAMETERS

Specifications	Value	Unit
Rated power P_{dm}	37	kW
Rated speed	1476	rpm
Rated torque factor M_{dm}	220.22	
Rated power factor $\cos\phi$	0.85	
Rated stator current I_{Idm}	71.8	A
Single phase stator resistor	0.049	Ω
Single phase reactance stator	0.0016	H
Single-phase rotor resistance (converted)	0.049	Ω
Single phase rotor reactance (converted)	0.0016	H
Moment of inertia	0.350	kgm ²
Engine performance	0.92	
Slip frequency	1.6 π	
Synchronization speed	1500	
Slip coefficient	0.016	
Stator time constant	0.475	
Time constant rotor	0.475	

Some typical working modes of the engine were surveyed through the following simulation scenario:

Magnetization occurs from 0 to 0.2 s, then the speed starts to change gradually from 0 rpm to the rated speed $\omega_{rated} = 1476$ rpm over the period from 0.2 s to 0.5 s. The blower load runs at a steady speed of $\omega_{dm} = 1476$ rpm for a period from 0.5 s to 1 s, and decelerates to 1000 rpm for from 1 s to 1.1 s. During the time interval from 1.1 s to 1.3 s, the speed stays the same at 1000 rpm, and starts to decrease to 0 rpm from 1.3 s to 1.5 s. The results we obtained met the requirements of the speed, flux and current controllers as seen in Figure 7. When comparing with the PI current controller in Figure 8, the precise linearization current controller offers lower overshoot and faster setup time than the PI current control.

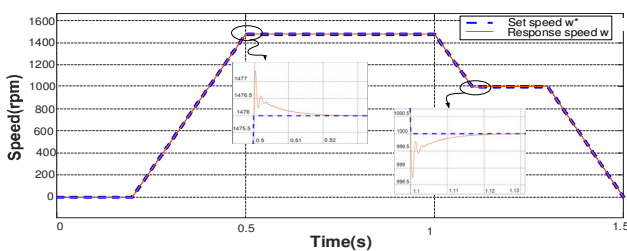


Fig. 7. Motor rotation speed response (FLC).

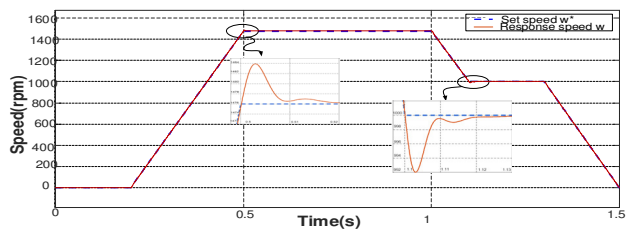


Fig. 8. Motor rotation speed response (PID).

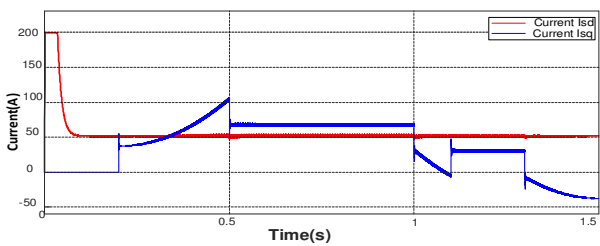


Fig. 9. Current I_{sd} , I_{sq} on dq .

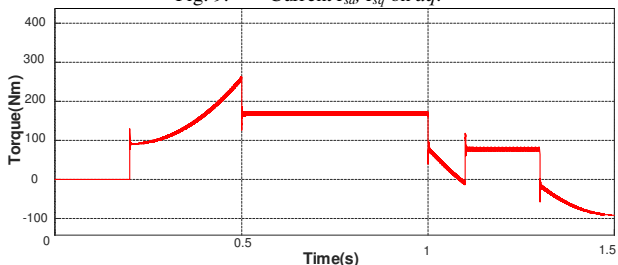


Fig. 10. Motor shaft end torque.

The controllers work quite accurately, the output follows the set value at the set time, the current regulator gives the

desired quick and accurate response, and the I_{sq} response has the same form as the output torque of the motor, as shown in Figures 9-10.

V. CONCLUSION

When using the precise calculation method for the power line, we get split channel between the axes d and q , so it was not necessary to construct a bidirectional current control table like in classical structural control, but it is possible to build separate controllers for the i_{sd} and i_{sq} components and surveying, analyzing, and synthesizing these controllers were performed according to the theory of control computation. Simulation test results on MATLAB/Simulink, confirmed the controller control calculations.

Simulations of the motor control scenario with speed levels resulted in a tracking speed response line with the set signal line, thus confirming that the current loop controller by the main linearization method can meet the fast, accurate, and recoupling requirements of the asynchronous motor current model. The speed response of the linearization method is better than that of the PID algorithm (The results of the speed response are compared in Figures 7 and 8).

The Thu Thiem road tunnel operates a Jet fan system in clusters at maximum capacity, so the control according to the speed levels of the Thu Thiem road tunnel jet fan is focused on energy saving. Because the vehicles circulate in the tunnel at varying quantities, depending on hour, day, weekends, or holidays, the concentration of exhaust gas and dust at each time is different, so it is possible to control the speed of the jet fan based on the concentration of the exhaust gases ensuring it is always at the allowable level.

ACKNOWLEDGMENT

We would like to thank the University of Transport and Communications for their support and the funding of this paper.

REFERENCES

- [1] A. Costantino, M. Musto, G. Rotondo, and A. Zullo, "Numerical Analysis for Reduced-scale Road Tunnel Model Equipped with Axial Jet Fan Ventilation System," *Energy Procedia*, vol. 45, pp. 1146–1154, Jan. 2014, <https://doi.org/10.1016/j.egypro.2014.01.120>.
- [2] V. Babrauskas *et al.*, "A methodology for obtaining and using toxic potency data for fire hazard analysis," *Fire Safety Journal*, vol. 31, no. 4, pp. 345–358, Nov. 1998, [https://doi.org/10.1016/S0379-7112\(98\)00013-7](https://doi.org/10.1016/S0379-7112(98)00013-7).
- [3] Y.-S. Choi, J.-H. Kim, K.-Y. Lee, and S.-H. Yang, "Performance Improvement of High Speed Jet Fan," *International Journal of Fluid Machinery and Systems*, vol. 3, no. 1, pp. 39–49, 2010, <https://doi.org/10.5293/IJFMS.2010.3.1.039>.
- [4] J.-H. Kim, J.-H. Kim, J.-Y. Yoon, Y.-S. Choi, and S.-H. Yang, "Application of multi-objective optimization techniques to improve the aerodynamic performance of a tunnel ventilation jet fan," *Proceedings of the Institution of Mechanical Engineers, Part C: Journal of Mechanical Engineering Science*, vol. 229, no. 1, pp. 91–105, Jan. 2015, <https://doi.org/10.1177/0954406214531566>.
- [5] L. Barbato, F. Cascetta, M. Musto, and G. Rotondo, "Fire safety investigation for road tunnel ventilation systems – An overview," *Tunnelling and Underground Space Technology*, vol. 43, pp. 253–265, Jul. 2014, <https://doi.org/10.1016/j.tust.2014.05.012>.

- [6] R. O. Carvel, A. N. Beard, P. W. Jowitt, and D. D. Drysdale, "Variation of heat release rate with forced longitudinal ventilation for vehicle fires in tunnels," *Fire Safety Journal*, vol. 36, no. 6, pp. 569–596, Sep. 2001, [https://doi.org/10.1016/S0379-7112\(01\)00010-8](https://doi.org/10.1016/S0379-7112(01)00010-8).
- [7] J.-H. Kim, J.-H. Kim, K.-Y. Kim, J.-Y. Yoon, S.-H. Yang, and Y.-S. Choi, "High-efficiency design of a tunnel ventilation jet fan through numerical optimization techniques," *Journal of Mechanical Science and Technology*, vol. 26, no. 6, pp. 1793–1800, Jun. 2012, <https://doi.org/10.1007/s12206-012-0420-9>.
- [8] A. Krol and M. Krol, "Transient Analyses and Energy Balance of Air Flow in Road Tunnels," *Energies*, vol. 11, no. 7, Jul. 2018, Art. no. 1759, <https://doi.org/10.3390/en11071759>.
- [9] Z. Tan, Z. Y. Huang, K. Wu, and L. T. Xu, "Theoretical Analysis of Longitudinal Ventilation System in a Road Tunnel for Predictive Control Based on Inertia Effect," *Advanced Materials Research*, vol. 639–640, pp. 665–669, 2013, <https://doi.org/10.4028/www.scientific.net/AMR.639-640.665>.
- [10] B. Chu, D. Hong, and J. Park, "Tunnel ventilation control via an actor-critic algorithm employing nonparametric policy gradients," *Journal of Mechanical Science and Technology*, vol. 23, no. 2, pp. 311–323, Feb. 2009, <https://doi.org/10.1007/s12206-008-0924-5>.
- [11] F. Tarada, R. Bopp, S. Nyfeler, K.-S. Jegal, and D.-S. Kim, "Ventilation and Risk Control of the Young Dong Rail Tunnel," in *First International Conference on Major Tunnel and Infrastructure Projects*, Taipei, Taiwan, Dec. 2000, pp. 1–10.
- [12] V. T. Ha, P. T. Giang, and V. H. Phuong, "T-Type Multi-Inverter Application for Traction Motor Control," *Engineering, Technology & Applied Science Research*, vol. 12, no. 2, pp. 8321–8327, Apr. 2022, <https://doi.org/10.48084/etasr.4776>.
- [13] N. H. Mugheri and M. U. Keerio, "An Optimal Fuzzy Logic-based PI Controller for the Speed Control of an Induction Motor using the V/F Method," *Engineering, Technology & Applied Science Research*, vol. 11, no. 4, pp. 7399–7404, Aug. 2021, <https://doi.org/10.48084/etasr.4255>.
- [14] R. Thangaraj, T. R. Chelliah, M. Pant, A. Abraham, and C. Grosan, "Optimal gain tuning of PI speed controller in induction motor drives using particle swarm optimization," *Logic Journal of the IGPL*, vol. 19, no. 2, pp. 343–356, Apr. 2011, <https://doi.org/10.1093/jigpal/jzq031>.
- [15] Y. Meng, B. Liu, and L. Wang, "Speed Control of PMSM Based on an Optimized ADRC Controller," *Mathematical Problems in Engineering*, vol. 2019, May 2019, Art. no. e1074702, <https://doi.org/10.1155/2019/1074702>.
- [16] E. H. E. Bayoumi and H. M. Soliman, "A particle swarm optimization-based deadbeat on-line speed control for sensorless induction motor drives," *Electromotion*, vol. 15, pp. 141–153, 2008.
- [17] N. H. Mugheri, M. U. Keerio, S. Chandio, and R. H. Memon, "Robust Speed Control of a Three Phase Induction Motor Using Support Vector Regression," *Engineering, Technology & Applied Science Research*, vol. 11, no. 6, pp. 7861–7866, Dec. 2021, <https://doi.org/10.48084/etasr.4476>.
- [18] T. L. Nguyen, T. H. Vo, and N. D. Le, "Backstepping Control for Induction Motors with Input and Output Constrains," *Engineering, Technology & Applied Science Research*, vol. 10, no. 4, pp. 5998–6003, Aug. 2020, <https://doi.org/10.48084/etasr.3680>.
- [19] R. N. Mishra and K. B. Mohanty, "Implementation of feedback-linearization-modelled induction motor drive through an adaptive simplified neuro-fuzzy approach," *Sadhana*, vol. 42, no. 12, pp. 2113–2135, Dec. 2017, <https://doi.org/10.1007/s12046-017-0741-6>.
- [20] C. Lascu, S. Jafarzadeh, M. S. Fadali, and F. Blaabjerg, "Direct Torque Control With Feedback Linearization for Induction Motor Drives," *IEEE Transactions on Power Electronics*, vol. 32, no. 3, pp. 2072–2080, Mar. 2017, <https://doi.org/10.1109/TPEL.2016.2564943>.
- [21] A. Devanshu, M. Singh, and N. Kumar, "Sliding Mode Control of Induction Motor Drive Based on Feedback Linearization," *IETE Journal of Research*, vol. 66, no. 2, pp. 256–269, Mar. 2020, <https://doi.org/10.1080/03772063.2018.1486743>.
- [22] B. Chu *et al.*, "GA-based fuzzy controller design for tunnel ventilation systems," *Automation in Construction*, vol. 17, no. 2, pp. 130–136, Jan. 2008, <https://doi.org/10.1016/j.autcon.2007.05.011>.
- [23] R. N. Mishra and K. B. Mohanty, "Real time implementation of an ANFIS-based induction motor drive via feedback linearization for performance enhancement," *Engineering Science and Technology, an International Journal*, vol. 19, no. 4, pp. 1714–1730, Dec. 2016, <https://doi.org/10.1016/j.jestch.2016.09.014>.
- [24] B. T. K. Hue, M. N. Thien, L. H. Thuong, H. T. Du, N. B. Nen, and H. T. Tuong, "A comparative study between input-output linearization control technique and backstepping control method for induction motor," *Journal of Technical Education Science*, vol. 64, pp. 48–56, 2021.
- [25] N. P. Quang and J.-A. Ditttrich, *Vector Control of Three-Phase AC Machines: System Development in the Practice*. New York, NY, USA: Springer, 2008.